Pakistan Veterinary Journal

ISSN: 0253-8318 (PRINT), 2074-7764 (ONLINE)
DOI: 10.29261/pakvetj/2026.134

RESEARCH ARTICLE

Bovine-Derived MRSA Bacteriophage vB_SauL_SHZU01: Study on Biological Characteristics, Genomics and Dairy Product Applications

Yaqian Liang[1#], Wenjing Wang[1#], Yulin Guo[1], Junkai Wang[1], Meihui Tian[1], Hui Zhang[1*] and Haihong Hao[1,2*]

[1]College of Animal Science and Technology, Shihezi University, Xinjiang 832000, China; [2]National Key Laboratory of Agricultural Microbiology Resources Exploration and Utilization, Huazhong Agricultural University, Hubei 430070, China. [#]These authors contributed equally.
*Corresponding author: 18409072772@163.com (HZ); haohaihong@aliyun.com (HH)

ARTICLE HISTORY (26-396)

Received: April 11, 2026
Revised: May 09, 2026
Accepted: May 10, 2026
Published online: May 25, 2026

Key words:
Bacteriophage
Biological properties
Bovine-derived MRSA
Control of antimicrobial-resistant bacteria
Dairy Product
Genome analysis

ABSTRACT

The abuse of antibiotics in the livestock and poultry industry has accelerated the spread of bovine-derived methicillin-resistant *Staphylococcus aureus* (MRSA), which not only endangers cattle health and reduces breeding efficiency but also threatens public health through the food chain. In this study, a lytic phage vB_SauL_SHZU01 targeting multidrug-resistant bovine-derived MRSA was isolated from dairy farm wastewater and systematically characterized. The phage had an icosahedral head and a long tail, belonging to the family Siphoviridae. It had an optimal multiplicity of infection (MOI) of 0.1, a short latent period of only 30 minutes, and strong infectivity. Its titer peaked at 37°C; it tolerated temperatures up to 50°C, remained infectious within pH 6-10, and showed time-dependent sensitivity to UV radiation. Whole-genome sequencing revealed that the phage contains a linear double-stranded DNA genome of 44,364 bp with a GC content of 33.6%. No antibiotic resistance genes were detected, but one anti-CRISPR protein-coding region was identified. Mouse experiments showed that 10^8–10^{10} CFU of this S. aureus strain caused 100% mortality in mice, while doses ≤10^7 CFU were non-lethal. The therapeutic effect of phage vB_SauL_SHZU01 was dose-dependent: it provided protection at ≥10^7 PFU, achieved 100% mouse survival at 10^8 PFU, and repaired liver, spleen, and kidney tissue damage caused by MRSA infection. In dairy product matrices, the phage effectively reduced the viable count of MRSA, and its antibacterial activity was synergistically regulated by temperature, matrix type, and MOI. In summary, phage vB_SauL_SHZU01 displays excellent lytic activity against multidrug-resistant bovine-derived MRSA. Systematic research on this phage provides a basis for understanding phage-host interactions and optimizing phage therapy, lays a technical foundation for the biological control of drug-resistant bacteria in livestock and poultry farming, and safeguards the safety of animal products and public health.

To Cite This Article: Liang Y, Wang W, Guo Y, Wang J, Tian M, Zhang H and Hao H, 2026. Bovine-derived mrsa bacteriophage vb_saul_shzu01: study on biological characteristics, genomics and dairy product applications. Pak Vet J, 46(6): 1387-1402. http://dx.doi.org/10.29261/pakvetj/2026.134

INTRODUCTION

Milk, as a global dairy raw material, plays a crucial role in the sustainable development of the dairy industry and human nutritional health (Velasco *et al.*, 2025). Its quality and safety are directly linked to both the viability of the dairy sector and public health. When contaminated by pathogenic bacteria, milk not only experiences a decline in quality, making it unfit for consumption, but also poses a serious risk to human health through the food chain. This contamination results in substantial economic losses to the global dairy industry each year (Phiri *et al.*, 2022). Among the various pathogenic bacteria that contaminate milk, *S. aureus* is one of the most significant, with its potential hazards affecting the entire "dairy cow breeding - milk production - human consumption" chain, thus warranting particular attention.

From the perspective of dairy cow breeding, *S. aureus* is the most prevalent pathogen responsible for mastitis in dairy cattle. It can colonize dairy cows, leading to both subclinical and clinical forms of mastitis (Guzmán-Luna *et al.*, 2022). Upon invading the mammary

glands, this bacterium not only threatens the health of dairy cows but also gives rise to two major issues: first, a substantial reduction in milk production, which diminishes overall production efficiency; second, the loss of essential nutritional components and failure to meet hygiene standards in the milk, compromising both the continuity and safety of milk production from the source and exacerbating economic losses within the dairy industry (Badawy *et al.*, 2022). Additionally, *S. aureus* can accelerate milk spoilage, degrade its natural quality and shelf life, and introduce further risks to milk storage and processing.

Furthermore, *S. aureus* can enter the food chain through contaminated milk, posing significant risks to human health. In addition to causing gastrointestinal diseases and skin and soft tissue infections, it can lead to more severe conditions, such as bacteremia, sepsis, and endocarditis in extreme cases, making it a major contributor to global foodborne outbreaks (Swets *et al.*, 2024). Currently, antibiotics remain the primary treatment for chronic bovine mastitis caused by *S. aureus*. However, the indiscriminate use of antibiotics in the breeding industry not only results in the accumulation of antibiotic residues in milk but also accelerates the emergence and spread of drug-resistant *S. aureus*, further exacerbating the dual threats to human health and the sustainable development of the dairy industry (Chambers *et al.*, 2024).

S. aureus can be classified into methicillin-sensitive *S. aureus* (MSSA) and methicillin-resistant *S. aureus* (MRSA) based on drug sensitivity characteristics. MSSA can evolve into MRSA by acquiring the staphylococcal cassette chromosome *mec* (SCCmec) element, which carries the mec gene. In contrast, MRSA exhibits broad-spectrum resistance to β-lactam antibiotics due to the presence of *mec* genes (such as *mecA*, *mecB*, and *mecC*), which encode the penicillin-binding protein 2a (PBP2a) (Wang *et al.*, 2018). Among these, MRSA carrying the *mecA* gene exhibits the most characteristic drug resistance. The emergence of multidrug-resistant (MDR) MRSA has further complicated prevention and control efforts (Abebe *et al.*, 2023; Leprince *et al.*, 2023). These drug-resistant strains not only significantly complicate the treatment of bovine mastitis, rendering traditional antibiotic-based control measures increasingly ineffective, but they also continue to pose a threat to human health through the food chain. This creates dual hazards, including the spread of antibiotic resistance genes, ecological safety risks, and food safety concerns. As a result, there is an urgent need to develop safe and effective alternative strategies for prevention and control (Wang *et al.*, 2023).

Bacteriophages (phages), viruses that specifically target and lyse bacteria, have re-emerged as a key area of research in the prevention and control of drug-resistant bacteria, particularly in the context of the growing issue of antibiotic resistance (Schooley *et al.*, 2024; Mobarezi *et al.*, 2025). Phages were used for the treatment of bacterial infections even before the advent of penicillin, and as antibiotic-resistant bacterial infections have become more widespread, phage therapy has once again garnered significant academic attention. The core advantages of phages include their narrow host range (which avoids disrupting the normal microbial flora), absence of residue risk, and ability to self-replicate. Furthermore, their clinical safety and natural abundance have been well-established, with some phage products being classified as "Generally Recognized as Safe (GRAS)" by the U.S. Food and Drug Administration (FDA) for controlling pathogenic bacterial contamination in food (Kim *et al.*, 2020; Nie *et al.*, 2025). While certain *S. aureus*-specific phages (e.g., LSA2308, KMSP1) have shown promise in food contamination control, research on phages specifically targeting bovine-derived MRSA remains relatively limited (Leprince *et al.*, 2023; Liu *et al.*, 2024).

In this study, we isolated and purified the phage vB_SauL_SHZU01, which targets bovine-derived MRSA, from dairy farm sewage. Its biological characteristics were analyzed using several methods, including the double-layer agar plate technique, one-step growth curve analysis, stability tests at various temperatures and pH levels, and transmission electron microscopy. Next-generation sequencing was used to analyze its whole-genome structure, genetic characteristics, and functional genes; meanwhile, *in-vivo* infection treatment experiments in mice were conducted to verify its therapeutic efficacy; and investigated the antibacterial activity and application safety of the phage in dairy products using raw milk and yogurt as matrices. Collectively, these experiments confirmed that vB_SauL_SHZU01 is a promising candidate for the prevention and control of bovine-derived MRSA. This study aims to provide a novel biological control resource for bovine mastitis caused by MRSA, contribute to the understanding of phage-host interactions, and offer a theoretical foundation for advancing the transformation of the aquaculture and livestock industries from "antibiotic dependence" to "green biological control," while ensuring the safety of livestock products and protecting public health.

MATERIALS AND METHODS

Isolation, purification and titration of phages vB_SauL_SHZU01: To isolate phages, this study used samples of dairy farm sewage, feces, and water trough water. Sewage and water trough water were centrifuged at 6,000 r/min for 30 min, filtered through gauze, and their supernatants were re-centrifuged; feces were dissolved in physiological saline with vortexing and treated identically. All supernatants were filtered through 0.22μM filters, and the filtrates were stored at 4°C. One clinically isolated multidrug-resistant *S. aureus* strains (NCBI AccessionPRJNA1417252): was used as host bacteria: after streaking on LB agar plates, single colonies were picked and shake-cultured to the logarithmic phase. A 200mL aliquot of filtrate was mixed with an equal volume of LB broth and 1mL of host bacteria, shake-cultured at 180 r/min for 12h, centrifuged, and the supernatant was filtered through a 0.22μM filter; phage-positive cultures were confirmed by the formation of circular, transparent plaques on double-layer agar plates, thus obtaining phage-containing broth. Phage isolation and purification were performed via the double-layer agar plate method: host bacteria and filtrate were mixed with LB semi-solid medium, poured onto plates, and transparent plaques were picked, treated and filtered. This process was repeated

until single phages with uniform morphology and size were obtained. Phage vB_SauL_SHZU01(NCBI: PX974351.1) was subjected to 10-fold serial dilution. Subsequently, 100μL of the diluted phage suspension was mixed with an equal volume of bacterial culture in the top agar. The resulting mixture was evenly plated onto the selection agar, which was then incubated at 37℃ for 10h. Phage titer was determined using the formula: phage titer = number of observed plaques×10×dilution factor.

Phage vB_SauL_SHZU01 morphology analysis: Transmission electron microscopy (TEM) was employed for the morphological characterization of phage vB_SauL_SHZU01, and the phage lysate used for TEM observation was pre-treated by gradient concentration to obtain a high-purity and high-concentration sample. For specific operations, the double-layer agar plate culture technique was used to cultivate the mixture of phage and host bacteria on the double-layer medium at the optimal multiplicity of infection (MOI) ratio, which was preliminarily determined through gradient MOI pre-experiments for the initial phage morphology analysis. This parameter ensures clear plaque morphology and the enrichment of a sufficient amount of phage particles, meeting the requirements for morphological observation. Subsequently, the culture plate was incubated overnight in a 37°C constant-temperature incubator, and a high-density phage suspension was finally obtained. Picking a single transparent plaque, it was co-cultured with log-phase host bacteria for phage propagation to improve the titer; after thoroughly rinsing the phages in the medium with SM buffer, the suspension was filtered through a 0.22μM filter membrane to obtain a phage lysate with a concentration of 10^8PFU/mL. The lysate was negatively stained with 2% phosphotungstic acid (w/v, pH 7.0). Finally, the morphological characteristics of the phage were observed using a HITACHI HT7800 transmission electron microscope (Hitachi, Ltd.), and micrographs were taken at an accelerating voltage of 80 kV to record the observation results. The size of the phage head and the length of its tail were measured using ImageJ software.

Determination of the optimal multiplicity of infection (MOI) of the phage vB_SauL_SHZU01: The multiplicity of infection (MOI) of a phage refers to the ratio of the initial number of phages (in PFU) to the number of host bacteria (in CFU). The optimal MOI is defined as the MOI at which the maximum number of phages is released under the same culture conditions. Phage suspensions and bacterial cultures, diluted to different concentrations, were mixed at MOI ratios of 100, 10, 1, 0.1 and 0.01, with 100μL of each added to 10mL of LB broth. The mixture was shake-incubated at 180r/min for 4h, then centrifuged at 6,000r/min for 10min. The supernatant was filtered through a 0.22μM filter, and the titer of the phage in the filtered solution was determined. The experiment was repeated three times, and the average value was calculated. Finally, a graph was plotted with different MOI values as the abscissa (x-axis) and the $\log_{10}$ value of the phage titer as the ordinate (y-axis).

One-Step growth curve of the phage vB_SauL_SHZU01: Phages were added to 20mL of LB broth containing *S. aureus* in the logarithmic growth phase at the optimal MOI. After inverting the mixture to ensure thorough mixing, it was incubated statically at 37°C for 10min, then centrifuged at 6,000r/min for 10min. The bacterial pellet was resuspended in 20mL of pre-warmed (37°C) LB broth; this centrifugation and resuspension process was repeated three times, with the supernatant discarded after each centrifugation step. Subsequently, the 20mL resuspended bacterial culture was incubated with shaking at 180r/min and 37°C, and timing started at 0min. From this point, 500μL samples were taken every 10min to determine the phage titer and the culture continued for a total of 150min. The experiment was repeated three times, and the average values were calculated. Based on this curve, the latent period, lysis period, and burst period of the phage during host infection were determined.

Thermal stability of the phage vB_SauL_SHZU01: Phage samples were aliquoted into 1mL portions. To determine the phage titer under different temperatures and time points, the aliquots were incubated at 0, 4, 25, 37, 50, 60 and 70°C, respectively with their titers measured at 10, 20, 30, 40, 50 and 60min. The experiment was repeated three times, and the average values were calculated.

pH Stability of the phage vB_SauL_SHZU01: The pH of LB broth was adjusted to 1, 2, 3, 4, 5, 6, 7, 8, 9, 10, 11, 12, 13 and 14 using HCl and NaOH solutions. LB broth with different pH values was aliquoted into 1.5mL EP tubes, and 100μL of phage suspension (10^8 PFU/mL) was added to each tube. After mixing thoroughly with a vortex mixer, the tubes were incubated in a 37°C metal bath for 1hour. Subsequently, the phage titer of each pH treatment group was determined. The experiment was repeated three times, and the average values were calculated.

UV sensitivity of the phage vB_SauL_SHZU01: 10 mL of phage culture was placed 20cM away from the UV lamp (254 nm) in a clean bench. The phage titer was determined at 10, 20, 30, 40, 50 and 60 min. The experiment was repeated three times, with the average values calculated.

***In-vitro* inhibition assay of the phage vB_SauL_SHZU01:** Phages and host bacteria were mixed at different multiplicities of infections (MOI = 100, 10, 1, 0.1, 0.01) and a control group (supplemented only with host bacteria) was set up simultaneously. The optical density (OD) of each group was measured at a wavelength of 600 nm (OD_{600}) every 1 hour, with continuous monitoring for 12 hours. The *in-vitro* inhibitory effect of the phage on host bacterial growth was analyzed based on the changes in OD_{600} values.

Experiment on phage-mediated control of biofilm formation: The biofilm formation experiment was conducted using a 96-well plate: 180μL of LB broth was added to each well, followed by 20μL of *S. aureus* bacterial suspension at a concentration of 10^8CFU/mL. The plate was incubated at 37°C for 24 hours to induce biofilm formation. After incubation, the medium containing planktonic bacteria in each well was gently

aspirated and discarded. The wells were washed with 1× PBS buffer to remove planktonic bacteria attached to the biofilm surface. Except for the control group, different concentrations of phage lysate (10^8, 10^7, 10^6, 10^5 and 10^4 PFU/mL) were added to the remaining wells. The 96-well plate was then incubated at 37°C for another 24 hours. After incubation, the phage lysate in each well was discarded and 1% crystal violet solution (w/v) was added to each well for staining, which lasted for 30 minutes. Excess dye was aspirated and discarded, and the residual dye in the wells was air-dried. Subsequently, 200μL of absolute ethanol was added to each well to dissolve the crystal violet bound to the biofilm. Finally, 100μL of the dissolved solution was transferred to a new 96-well polystyrene plate, and the absorbance was measured at a wavelength of 595nM to evaluate the amount of biofilm formed.

Whole-genome analysis of the phage vB_SauL_SHZU01: In this study, the VAHTS® Universal Plus DNA Library Prep Kit for MGI V2/for Illumina V2 was used to construct the whole-genome library of phage vB_SauL_SHZU01, and sequencing was performed using the NovaSeq 6000 platform (Illumina, USA). Filter low-quality reads and trim adapters using Trimmomatic (v0.4). For gene assembly, SPAdes software was employed for sequence spades, with concurrent removal of host bacterial contaminating sequences. After assembly, genomic data were annotated using Prokka v1.14.6 software. The phage genome was annotated using PhageScope, which is an online tool specifically designed for phage genome annotation. PhageScope integrates multiple bioinformatics pipelines, including BLASTx 2.15.0 searches against phage-specific databases (PHROGs, Uniprot, Pfam), conserved domain identification, and structural protein prediction. Antimicrobial resistance genes (ARGs) were predicted using ResFinder v4.6.0 under default threshold parameters. For the prediction of virulence-associated genes (VAGs), ABRicate v1.0.1 software (https://github.com/tseemann/abricate) was utilized with default thresholds under the VFDB (Virulence Factor Database) configuration. Additionally, prophage segments were predicted and their sequences extracted using Phigaro v2.4.0 in basic mode.

***In-vivo* bacteriostatic experiment in mice:** A total of 72 Kunming mice (6-8 weeks old, body weight: 30.13 ± 2.39 g) were selected, with half male and half female. This experiment was divided into two parts: In the first part, 42 mice (half male and half female) were used. This study was conducted with ethics approval number A2025-1204. Each mouse was given an intraperitoneal injection of 200μL *S. aureus* suspensions at different concentrations (10^{10}, 10^9, 10^8, 10^7, 10^6 and 10^5CFU) into the left abdomen; meanwhile, a normal saline control group was set up (mice in this group were injected with 200μL normal saline into the left abdomen). The survival status of the mice was observed continuously. In the second part, 36 mice were used. The phage was intraperitoneally injected 30 minutes after the intraperitoneal injection of *S. aureus.* First, 200μL of *S. aureus* suspension at a concentration of 10^8CFU was injected into the left abdomen of each mouse (note: all mice in the 10^8CFU *S. aureus* group died within 24h, while all mice in the 10^7CFU *S. aureus* group remained healthy and alive). A bacteriophage control group was set up, where each mouse was injected with 200μL of bacteriophage suspension at 10^8CFU without *S. aureus* injection. Then, 200μL of bacteriophage suspensions at different concentrations (10^8, 10^7, 10^6, 10^5 and 10^4CFU) was injected into the right abdomen of each mouse. The survival status and mental state of the mice were observed continuously. At 3 days and 7 days after bacteriophage injection, the liver, kidney, and spleen of the surviving mice were collected for section preparation. Hematoxylin-eosin (HE) staining was performed on these tissue sections, and their morphological characteristics were observed.

Antibacterial activity of phage vB_SauL_SHZU01 in dairy products: In this experiment, commercially available liquid dairy products (row milk, yogurt) from Shihezi, Xinjiang, were selected as research matrices. Pasteurized fresh milk is a liquid with strong fluidity, while yogurt is a liquid with thick texture, and the yogurt used in this experiment contains no probiotic strains after cultivation. For the treatment of liquid dairy products, 100mL of fresh cow's milk and 100mL of probiotic yogurt was placed in sterile Erlenmeyer flasks. To each flask, 1mL of *S. aureus* bacterial suspension with a concentration of 1×10^7CFU/mL was added, followed by shaking to mix evenly for uniform distribution of the pathogenic bacteria. Subsequently, phage vB_SauL_ SHZU01 was inoculated into the flasks, so that the multiplicity of infection (MOI) of the system reached 100,10, 1, 0.1 and 0.01, respectively. All experimental groups were set with three temperature treatment groups: 4, 25 and 37°C. Starting from 0 h of co-incubation of the phage and pathogenic bacteria, samples were taken for detection every 3h. For liquid samples: 1mL of the system solution was taken, and the number of viable *S. aureus* was determined by the plate counting method after serial dilution. Continuous monitoring was conducted for 24h, and the number of viable pathogenic bacteria at different time points was recorded in units of CFU/mL, to analyze the differences in the antibacterial activity of the phage under different dairy matrices, temperatures, and MOI conditions. Meanwhile, based on the above experimental system, the application safety of the phage in milk was evaluated from three core dimensions: phage host specificity, phage compatibility with milk matrix, and safety of applied concentration, with all evaluation methods carried out based on the existing experimental design and previous biological identification results.

Statistical analysis: All experimental data in this study were statistically analyzed using WPS software, and the experimental results were expressed as mean ± standard deviation (Mean±SD). Differences among multiple groups were examined by one-way analysis of variance (one-way ANOVA), with $P<0.05$ considered to denote a statistically significant difference. Graphing was performed using Origin 2024, and image assembly and format optimization were completed using Adobe Illustrator 2025.

RESULTS

Isolation, purification, and morphology of phage vB_SauL_SHZU01: A lytic phage targeting multidrug-resistant *S. aureus* was isolated from the wastewater of a cattle farm in Shihezi, Xinjiang, using an appropriate selection medium. After purification, this phage was named vB_SauL_SHZU01. When *S. aureus* was used as the host bacterium and relevant experiments were conducted on a double-layered agar, the phage formed transparent plaques with a diameter of less than 1mM (Fig. 1A). Transmission Electron Microscopy (TEM) analysis revealed that phage vB_SauL_SHZU01 exhibits the typical morphological characteristics of an icosahedral head and a non-contractile tail belonging to the order Caudoviricetes and family Siphoviridae. Its head presents a spherical icosahedral symmetric structure, with a size of 63.79 ± 2.86nM. The phage has a non-contractile tail, which measures 249.52 ±0.99nM in length (Fig. 1B).

Biological characteristics of phage vB_SauL_SHZU01: The titer reached a peak (2.8×10^8PFU/mL) when the MOI was 0.1 (Fig. 2A). In terms of temperature stability, phage vB_SauL_SHZU01 exhibited relatively stable tolerance within the temperature range of 4 to 50℃. When the temperature increased to 60℃, its titer gradually decreased, and a more significant rate of titer reduction was observed as the temperature further rose to 70℃ (Fig. 2B). Additionally, phage vB_SauL_SHZU01 showed no activity within the pH ranges of 1-4 and 11-14, while maintaining strong activity in the pH range of 6-10, indicating that this phage has a narrow pH adaptation range with a preference for neutral environments (Fig. 2C). As the ultraviolet (UV) irradiation time extended from 0 to 60 minutes, the phage titer (expressed as $\log_{10}$(PFU/mL)) showed a gradual decreasing trend. The initial titer (at 0 minutes) was approximately $\log_{10}$(PFU/mL) 7.3, and it decreased to approximately $\log_{10}$(PFU/mL) 5.9 by 60 minutes (Fig. 2D). This indicates that the activity of the phage gradually diminished with prolonged UV exposure, suggesting poor UV stability. UV radiation caused damage to the phage, with longer irradiation times resulting in more significant damage and fewer surviving phages.

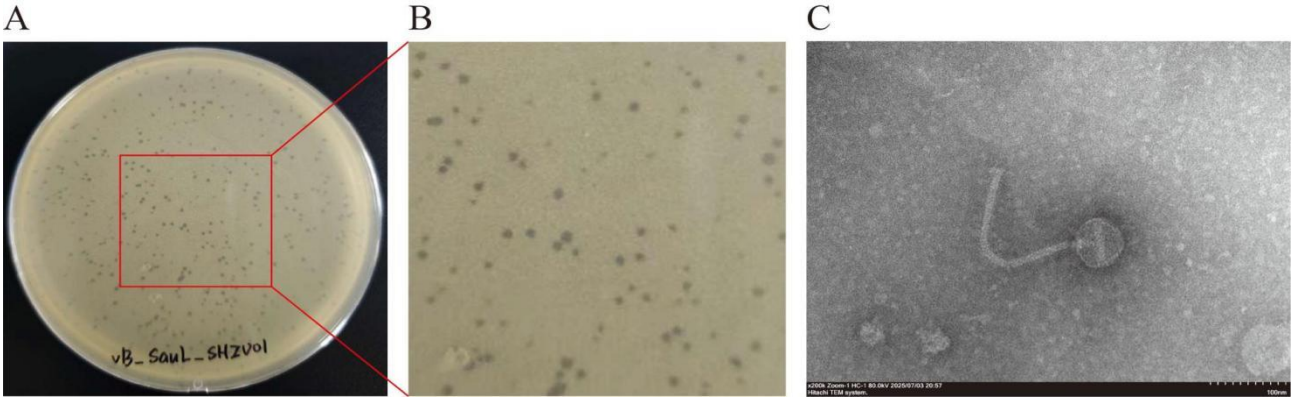

Fig. 1: Morphological characteristics of vB_SauL_SHZU01. (A) Plaque morphology on the whole double-layer agar plate. (B) High-resolution plaque morphology on the double-layer agar plate. (C) Morphology of phage vB_SauL_SHZU01 under transmission electron microscopy (scale bar = 100 nm).

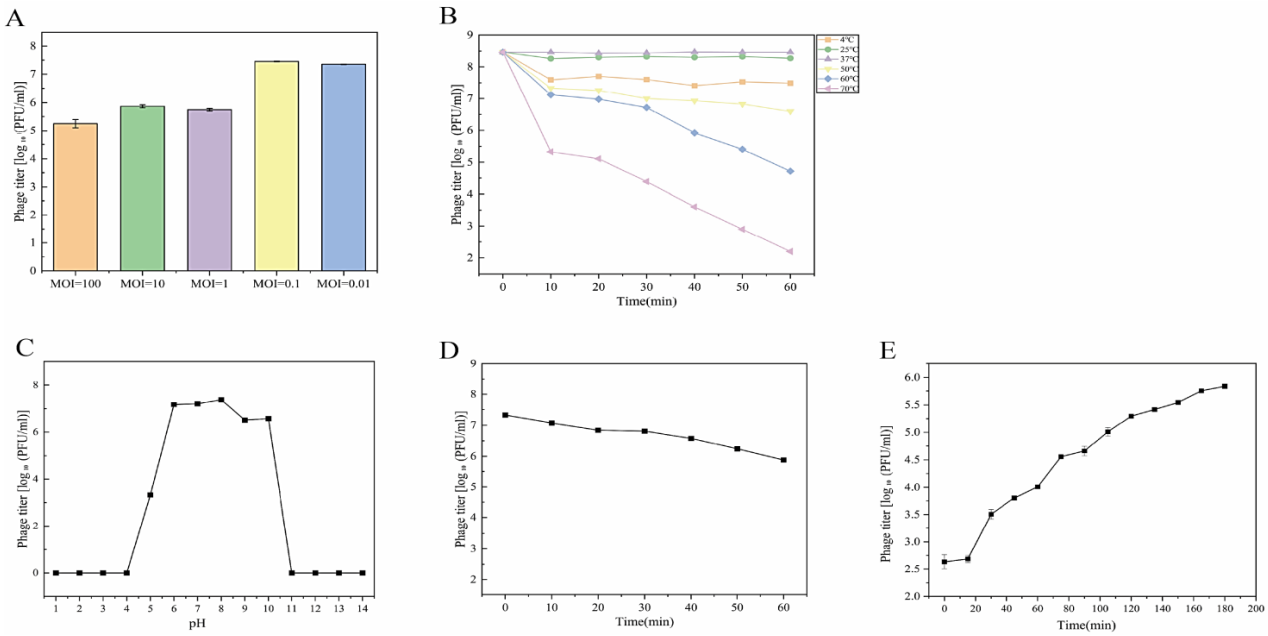

Fig. 2: Biological characteristics of phage vB_SauL_SHZU01. (A) Optimal multiplicity of infection (MOI) of phage vB_SauL_SHZU01; (B) Temperature stability of phage vB_SauL_SHZU01; (C) pH stability of phage vB_SauL_SHZU01; (D) UV sensitivity of phage vB_SauL_SHZU01; (E) One-step growth curve of phage vB_SauL_SHZU01.

Experimental data demonstrated that different multiplicities of infection (MOI) significantly affected the infection efficiency of the phage. Accordingly, an MOI of 0.1 was selected to determine the one-step growth curve of phage vB_SauL_SHZU01 (Fig. 2E). The results showed that vB_SauL_SHZU01 remained in the latent period from approximately 0 to 20 minutes, with the titer remaining relatively stable at log_{10}(PFU/mL) 2.6-2.7. It entered the lytic phase from 20 to 80 minutes, during which the titer increased rapidly, reaching log_{10}(PFU/mL) 4.5 at 80 minutes. After 80 minutes, it entered the stationary phase, with the titer continuing to rise slowly and stabilizing at approximately log_{10}(PFU/mL) 5.8 by 180 minutes. These findings indicate that the phage possesses short latent and lytic periods, enabling efficient proliferation and release of a large number of progeny phages.

The lytic performance of phage vB_SauL_SHZU01 on the host strain: To evaluate the lytic activity of the bacteriophage, *S. aureus* SHZU01 was used as the host bacterium. Compared with the phage-free control group, the bacteriophage could effectively lyse the bacterial biofilm. At multiplicities of infection (MOI) of 100, 10, 1, 0.1, and 0.01, the OD_{600} value of the bacterial biofilm decreased gradually with the reduction of MOI (Fig. 3A). Among these MOI values, the lytic effect was most significant when MOI = 0.01, indicating that the lytic effect of the bacteriophage on the bacterial biofilm enhanced as the MOI decreased. The *in-vitro* bacteriostatic assay revealed a distinct MOI-dependent inhibitory effect of the phage on *S. aureus* growth (Fig. 3B): a higher MOI conferred a stronger bacterial growth delay, while a lower MOI led to earlier growth initiation and a faster proliferation rate. For the high-MOI group (MOI=100, 10), bacterial growth was markedly delayed, with the OD_{600} value remaining low in the early phase (8h for MOI=100, 7h for MOI=10). Rapid proliferation occurred only in the late phase (after 8h for MOI=100, 7h for MOI=10) and the OD_{600} value reached that of the pure culture group at 12–13h (capped at 3.0 by the instrument detection limit). In the medium-MOI group (MOI=1, 0.1), growth initiated earlier than the high-MOI group (6–7h for MOI=1, 5–6h for MOI=0.1), with accelerated proliferation approaching the instrument detection limit at ~10h (MOI=1) and 9–10h (MOI=0.1), respectively. The low-MOI group (MOI=0.01, 0.001, 0.0001) exhibited further attenuation of the phage's inhibitory effect, with even earlier growth initiation (4–5h for MOI=0.01, 3–4h for MOI=0.001, 2–3h for MOI=0.0001). Additionally, a lower MOI correlated with a faster proliferation rate and an earlier time to reach a high OD_{600} value; for instance, a prominent proliferation peak was observed at 3–4 h when MOI=0.0001.

Whole-genome sequencing results: Next-generation sequencing (NGS) was performed on phage vB_SauL_SHZU01. After filtering the raw data, 590,897,380 bp of clean sequencing data was obtained, with a Q20 rate of 98.910%, a Q30 rate of 95.907%, and a GC content of 33.576%. The data quality was good and could meet the requirements of subsequent analyses. De novo genome assembly was conducted on the filtered data using Unicycler software, yielding one contig with a length of 44,364 bp and a GC content of 33.6% (Fig. 4A). Gene prediction of the assembled phage genome was carried out using Prokka software and a total of 62 genes were predicted (Fig. 4B), with a total length of 41,262 bp and an average length of 666 bp, accounting for 93.01% of the total genome length. These included 61 coding sequences (CDSs) with a total length of 41,112 bp and an average length of 674 bp, and 1 misc RNA with a length of 150 bp; no tRNA or rRNA was predicted. Six pseudogenes were identified using Pseudofinder software, with a total length of 1,365 bp and an average length of 227.5 bp. Repetitive sequence analysis showed that the total amount of repetitive sequences in the phage genome was small, with 3 repetitive sequences detected (total length 124 bp, coverage rate only 0.28%), mainly including 1 LINE type and 2 simple repeat sequences. No prophage sequences were detected, suggesting that it may be a virulent phage.

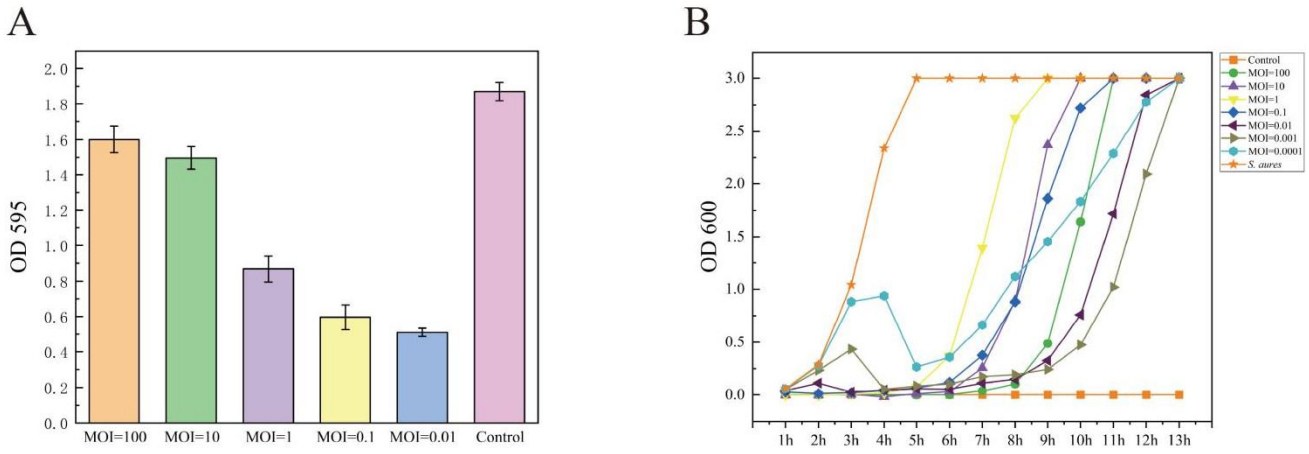

Fig. 3: Lytic effect of phage vB_SauL_SHZU01 on biofilm and its *in-vitro* inhibitory effect on the growth of *S. aureus* SHZU01. (A) Lytic effect of phage vB_SauL_SHZU01 on the biofilm of *S. aureus* SHZU01 (measured at OD595 nm); (B) *In-vitro* inhibitory effect of phage vB_SauL_SHZU01 on the growth of *S. aureus* SHZU01 (measured at OD600 nm).

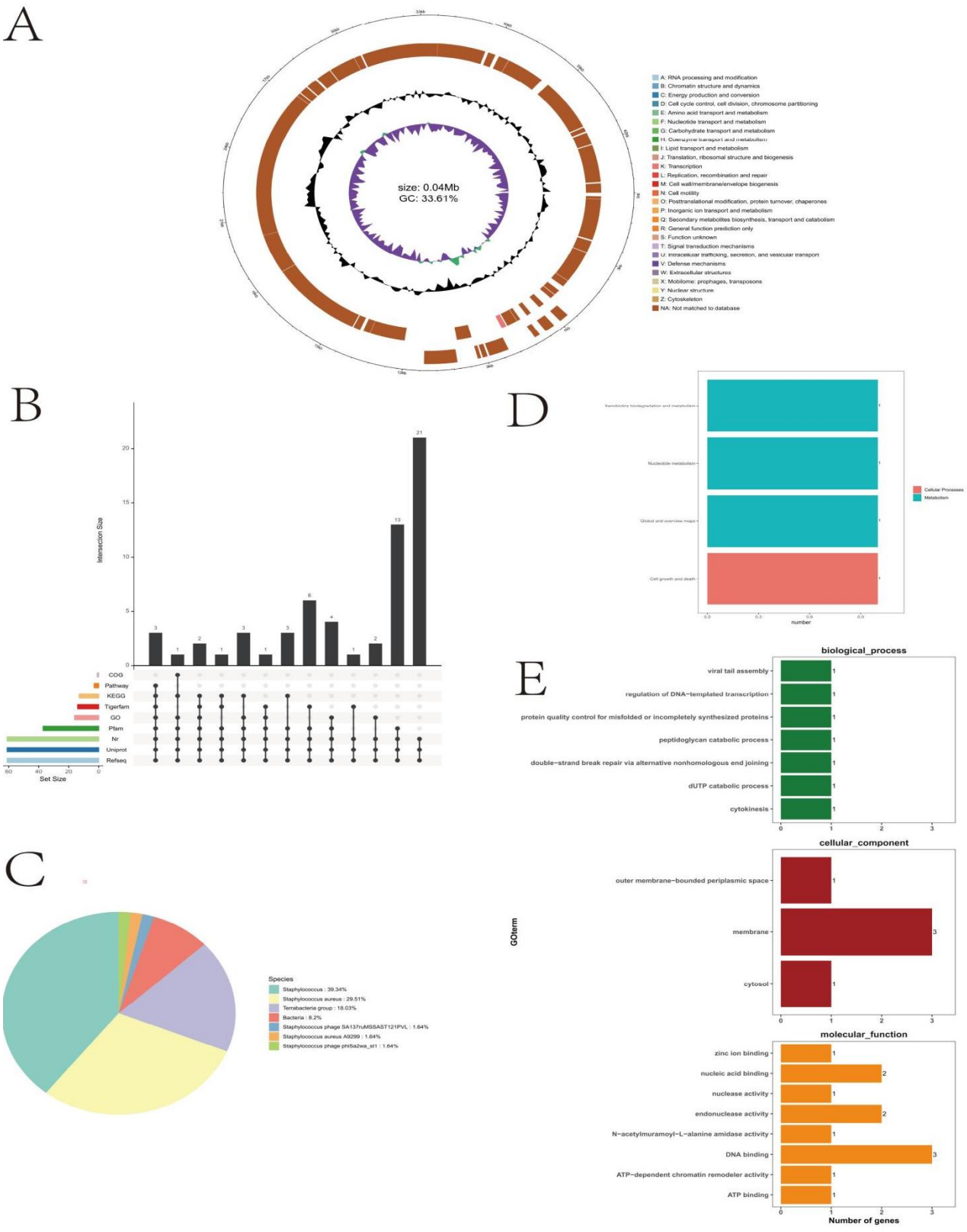

Fig. 4: Related analysis results of the phage vB_SauL_SHZU01 genome. (A) Genome circle map of the phage vB_SauL_SHZU01; (B) Statistical Chart of Common and Specific Annotations of Coding Genes in General Databases. The left side shows the statistical results of gene annotations in general databases; the right side shows the statistics of common and specific annotations. For example, the first column represents the statistical situation of annotations common to all general databases, the upper part shows the statistics of the number of genes, and the lower part shows the labels of common or specific databases; (C) NR species distribution map, where different colors represent different species; (D) KEGG database annotation table, in which SeqID is the gene ID given by Prokka software annotation, A and B are the secondary classifications of ko pathway respectively, C is the annotation information corresponding to the ko number, and PathwayID is the ko number; (E) GOslim classification statistical chart. This chart is obtained by simplifying the Gene Ontology (GO) annotation information. The gene functions are summarized and counted from three dimensions: cellular component, molecular function, and biological process. The top 20 GOslim secondary classifications with the most annotations in each dimension are selected for plotting. The abscissa is the content of each GO secondary classification, and the ordinate is the number of genes in the corresponding classification. This chart is used to show the gene enrichment status of each GO secondary function under the background of all genes, and clarify the status of each secondary function in the phage genome.

To clarify the functions of phage genes, the predicted 61 CDS sequences were annotated against general and specialized databases, and the coding genes were aligned with 8 general functional databases (Table 1). The results of general database annotation showed that all CDSs obtained at least one type of database annotation, among which the annotation rates of Nr, Uniprot and Refseq databases were all 100%. The NR species distribution results indicated that the genes in the phage genome had high homology with species related to the genus Staphylococcus, further verifying the host relevance of the phage (Fig. 4C). In addition, different degrees of annotation were observed in the Pfam (37, 60.66%) (Table 2), TIGRFAMs (14, 22.95%) (Table 3), KEGG (13, 21.31%) (Fig. 4D), GO (16, 26.23%) (Fig. 4E), and COG (1, 1.64%) databases. A total of 14 genes were annotated in the TIGRFAMs database, mainly including transcriptional repressor LexA, tyrosine recombinases XerC/XerD, N-acetylmuramoyl-L-alanine amidase CwlD, phage holin, phage tail tape measure protein, phage major tail protein, head-tail connector protein, and phage major capsid protein. These genes are closely related to the infection, replication, assembly and lysis functions of the phage. In the virulence-related annotation, the Virulence Factors Database (VFDB) clearly annotated 2 virulence-related genes, namely the *fimB* gene (encoding a type 1 fimbriae regulatory protein, associated with bacterial adhesion virulence) and the *clpP* gene (encoding an ATP-dependent Clp protease proteolytic subunit, associated with bacterial stress survival virulence). The Pathogen Host Interactions (PHI) database annotated 4 virulence-related genes, including ctg_00021 (PhiID: 123245, associated with Streptococcus suis virulence, with reduced virulence after mutation), ctg_00033 (PhiID: 7198, associated with *Campylobacter jejuni*, with loss of pathogenicity after mutation), ctg_00043 (PhiID: 124329, associated with *Brucella abortus*, with reduced virulence after mutation), and ctg_00049 (PhiID: 10379, associated with *Verticillium dahliae*, with reduced virulence after mutation). In addition, 3 type III secretion system (T3SS) effector proteins (ctg_00052, ctg_00008, ctg_00057) were predicted by EffectiveT3 software, all of which were hypothetical proteins. No related genes were annotated in the ARDB, CARD, CYP450, and CAZy databases. Signal peptide and transmembrane protein prediction showed 1 signal peptide protein and 5 transmembrane proteins, with no secreted proteins. Multiple membrane transport protein-related genes were annotated in the TCDB database.

***In-vivo* bacteriostatic experiment of bacteriophage in mice:** To investigate the lethal effect of *S. aureus* strain SHZU01 on mice, this study employed an *in-vivo* injection approach. Each mouse was injected with 1×10^n CFU (where n = 10, 9, 8, 7, 6, 5, 4) of *S. aureus* SHZU01 bacterial suspension, with 7 bacterial concentration treatment groups established (concentration range: 10^{10} to 10^4CFU) and 6 mice per group. A blank control group was also included, where mice received an equal volume of sterile solvent (*i.e.*, normal saline). Mice were continuously observed for 7 days, with the number of surviving mice in each group recorded daily. The results showed that no mice survived within 24 hours of the experiment's initiation in the high-concentration groups (10^{10} to 10^8CFU). In contrast, all mice in the 10^7 to 10^4 CFU concentration groups and the blank control group survived (100% survival rate) over the 7-day period (6/6 mice). Mice injected with a single dose of 10^8 PFU phage alone remained healthy throughout the observation period, with no abnormal clinical signs, and pathological examination of their organs revealed no obvious pathological changes.

Table 1: Statistics of coding gene annotation results

Item	Count	Percentage
All	61	100.00
Annotation	61	100.00
KEGG	13	21.31
Pathway	3	4.92
Nr	61	100.00
Uniprot	61	100.00
GO	16	26.23
COG	1	1.64
Pfam	37	60.66
Refseq	61	100.00
Tigerfam	14	22.95

Note: In the first column, All refers to all genes; Annotation refers to genes with at least one type of annotation; KEGG refers to genes annotated to the KEGG database; Pathway refers to genes annotated to the KEGG Pathway database; Nr refers to genes annotated to the Nr database; Uniprot refers to genes annotated to the Uniprot database; GO refers to genes annotated to the GO database; COG refers to genes annotated to the COG database; Pfam refers to genes annotated to the Pfam database; Refseq refers to genes annotated to the Refseq database; Tigrfam refers to genes annotated to the Tigrfams database; the second column shows the corresponding number of each Item; the third column shows the corresponding proportion of each Item.

In the phage treatment experiment for *S. aureus*-infected mice, *S. aureus* at a concentration of 10^8 CFU was used to infect the mice, which were then treated with phage vB_SauL_SHZU01 at concentrations of 1×10^n PFU (where n = 8, 7, 6, 5, 4). The phage displayed a clear concentration-dependent effect in rescuing the infected mice: a rescuing effect was only observed when its concentration reached 10^7 PFU or higher. Specifically, phage at 10^8 PFU resulted in 100% survival of the mice (optimal rescuing effect), while phage at 10^7 PFU only provided partial protection. No rescuing ability was observed when the phage concentration was $\leq 10^6$ PFU.

Hematoxylin-eosin (HE) staining was performed to evaluate histopathological changes in the liver, spleen, and kidneys of *S. aureus*-infected mice at 3 days (3d) and 7 days (7d) post-treatment with phage vB_Sau_SHZU01 (Fig. 5).

In the control group, liver lobule structure was intact, with hepatic cords radially and orderly arranged around the central vein. Hepatocytes exhibited regular morphology and homogeneous cytoplasm, with no hepatocellular degeneration, necrosis, or inflammatory cell infiltration detected. At 3 days post-phage treatment, the 10^7PFU group showed diffuse hepatocellular swelling, focal hemorrhage in some areas, and ballooning or acidophilic degeneration in some hepatocytes, accompanied by a small number of neutrophils infiltrating the liver lobules and portal areas. In the 10^8 PFU group, although hepatocellular edema and focal hemorrhage were present, the lesion extent and cellular damage were less severe than those in the 10^7 PFU group. By 7 days post-treatment, histopathological damage in the 10^8PFU group was significantly alleviated: liver lobule structure was

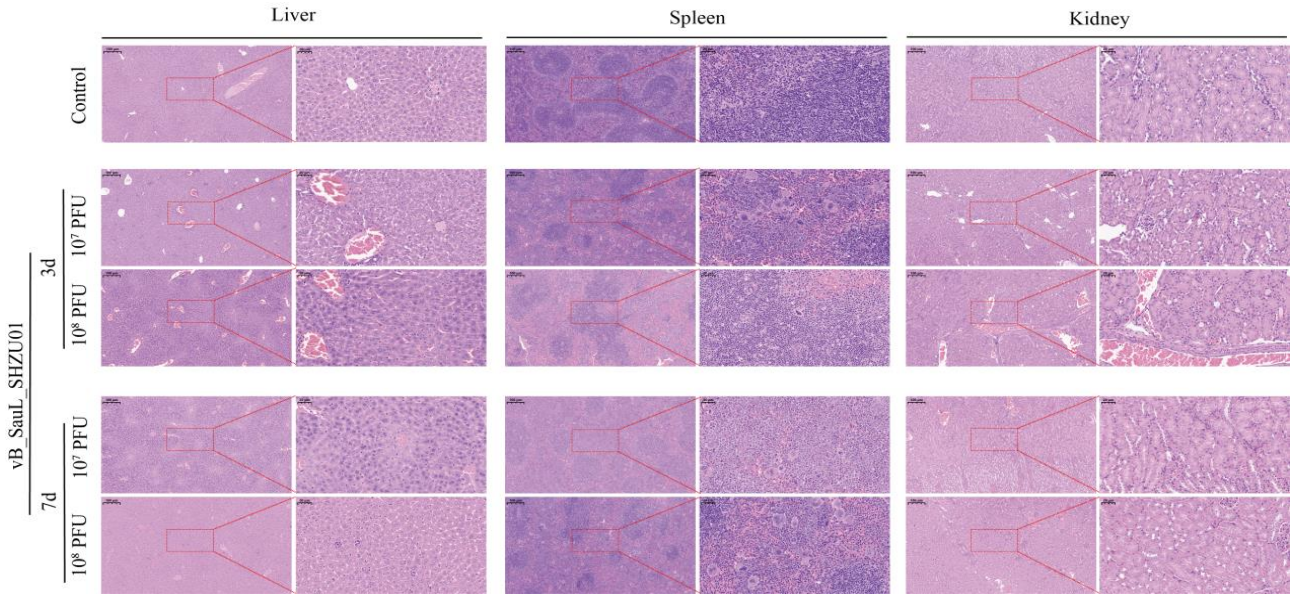

Fig. 5: Tissue sections of liver, spleen and kidney from mice infected with different concentrations of phage vB_SauL_SHZU01 at 3 days (3 d) and 7 days (7 d) post-infection.

Table 2: PFAM Domain annotation

SeqID	Accession	HMMProfile	Description	SeqID
ctg_00002	PF00476.25	DNA_pol_A	DNA polymerase family A	ctg_00002
ctg_00003	PF10991.13	Enc34_ssDNA-bd	Enterobacter phage Enc34, ssDNA-binding protein	ctg_00003
ctg_00004	PF10926.13	DUF2800	Protein of unknown function (DUF2800)	ctg_00004
ctg_00004	PF12705.12	PDDEXK_1	PD-(D/E)XK nuclease superfamily	ctg_00004
ctg_00007	PF13384.11	HTH_23	Homeodomain-like domain	ctg_00007
ctg_00010	PF11195.13	DUF2829	Protein of unknown function (DUF2829)	ctg_00010
ctg_00011	PF10711.14	DUF2513	Hypothetical protein (DUF2513)	ctg_00011
ctg_00016	PF13443.11	HTH_26	Cro/C1-type HTH DNA-binding domain	ctg_00016
ctg_00016	PF01381.27	HTH_3	Helix-turn-helix	ctg_00016
ctg_00017	PF12844.12	HTH_19	Helix-turn-helix domain	ctg_00017
ctg_00017	PF01381.27	HTH_3	Helix-turn-helix	ctg_00017
ctg_00017	PF00717.28	Peptidase_S24	Peptidase S24-like	ctg_00017
ctg_00021	PF00589.27	Phage_integrase	Phage integrase family	ctg_00021
ctg_00023	PF05257.21	CHAP	CHAP domain	ctg_00023
ctg_00023	PF01520.23	Amidase_3	N-acetylmuramoyl-L-alanine amidase	ctg_00023
ctg_00023	PF08460.15	SH3_5	Bacterial SH3 domain	ctg_00023
ctg_00024	PF04688.18	Holin_SPP1	SPP1 phage holin	ctg_00024
ctg_00025	PF11166.13	DUF2951	Protein of unknown function (DUF2951)	ctg_00025
ctg_00026	PF09693.15	Phage_XkdX	Phage uncharacterised protein (Phage_XkdX)	ctg_00026
ctg_00027	PF11192.13	DUF2977	Protein of unknown function (DUF2977)	ctg_00027
ctg_00028	PF10651.14	BppU_N	BppU N-terminal domain	ctg_00028
ctg_00029	PF21311.2	Phage_RBD_prop	Phage 5-bladed beta propeller receptor binding platform domain	ctg_00029
ctg_00031	PF18994.5	Prophage_tailD1	Prophage endopeptidase tail N-terminal domain	ctg_00031
ctg_00031	PF06605.16	Prophage_tail	Prophage endopeptidase tail	ctg_00031
ctg_00032	PF05709.16	Sipho_tail	Phage tail protein RIFT-related domain	ctg_00032
ctg_00033	PF10145.14	PhageMin_Tail	Phage-related minor tail protein	ctg_00033
ctg_00033	PF01551.27	Peptidase_M23	Peptidase family M23	ctg_00033
ctg_00036	PF02368.23	Big_2	Bacterial Ig-like domain (group 2)	ctg_00036
ctg_00037	PF04630.17	Phage_TTP_1	Phage tail tube protein	ctg_00037
ctg_00041	PF05135.18	Phage_connect_1	Phage gp6-like head-tail connector protein	ctg_00041
ctg_00042	PF05065.18	Phage_capsid	Phage capsid family	ctg_00042
ctg_00043	PF00574.28	CLP_protease	Clp protease	ctg_00043
ctg_00044	PF04860.17	Phage_portal	Phage portal protein	ctg_00044
ctg_00045	PF03354.20	TerL_ATPase	Terminase large subunit, ATPase domain	ctg_00045
ctg_00045	PF20441.3	TerL_nuclease	Terminase large subunit, endonuclease domain	ctg_00045
ctg_00046	PF05119.17	Terminase_4	Phage terminase, small subunit	ctg_00046
ctg_00047	PF01844.28	HNH	HNH endonuclease	ctg_00047
ctg_00049	PF00270.34	DEAD	DEAD/DEAH box helicase	ctg_00049
ctg_00049	PF00176.28	SNF2-rel_dom	SNF2-related domain	ctg_00049
ctg_00051	PF05272.16	VapE-like_dom	Virulence-associated protein E-like domain	ctg_00051
ctg_00052	PF07438.16	DUF1514	Protein of unknown function (DUF1514)	ctg_00052
ctg_00053	PF06116.17	RinB	Transcriptional activator RinB	ctg_00053
ctg_00054	PF07129.16	DUF1381	Protein of unknown function (DUF1381)	ctg_00054
ctg_00056	PF00692.24	dUTPase	dUTPase	ctg_00056
ctg_00057	PF06260.17	DUF1024	Protein of unknown function (DUF1024)	ctg_00057
ctg_00061	PF06194.16	Phage_Orf51	Phage Conserved Open Reading Frame 51	ctg_00061
ctg_00062	PF07768.16	PVL_ORF50	PVL ORF-50-like family	ctg_00062

Note: SeqID: The ID of the gene number assigned during Prokka software annotation; Accession: PF number, a stable and unique identifier for each family; HMMProfile: Domain; Description: Description information.

Table 3: TIGRFAMs Domain Annotation

SeqID	Accession	HMMProfile	Description
ctg_00017	TIGR00498.1	lexA	JCVI: transcriptional repressor LexA
ctg_00021	TIGR02224.1	recomb_XerC	JCVI: tyrosine recombinase XerC
ctg_00021	TIGR02225.1	recomb_XerD	JCVI: site-specific tyrosine recombinase XerD
ctg_00023	TIGR02883.1	spore_cwlD	JCVI: N-acetylmuramoyl-L-alanine amidase CwlD
ctg_00024	TIGR01592.1	holin_SPP1	JCVI: phage holin
ctg_00026	TIGR01669.1	phage_XkdX	JCVI: XkdX family protein
ctg_00033	TIGR01760.1	tape_meas_TP901	JCVI: phage tail tape measure protein
ctg_00037	TIGR01603.1	maj_tail_phi13	JCVI: phage major tail protein, phi13 family
ctg_00041	TIGR01560.2	put_DNA_pack	JCVI: head-tail connector protein
ctg_00042	TIGR01554.3	major_cap_HK97	JCVI: phage major capsid protein, HK97 family
ctg_00043	TIGR00706.1	SppA_dom	JCVI: signal peptide peptidase SppA
ctg_00043	TIGR00493.1	clpP	JCVI: ATP-dependent Clp endopeptidase proteolytic subunit ClpP
ctg_00044	TIGR01537.1	portal_HK97	JCVI: phage portal protein
ctg_00046	TIGR01558.1	sm_term_P27	JCVI: phage terminase small subunit P27 family
ctg_00048	TIGR01636.1	phage_rinA	JCVI: phage transcriptional regulator, RinA family
ctg_00056	TIGR00576.1	Dut	JCVI: dUTP diphosphatase
ctg_00056	TIGR02274.1	dCTP_deam	JCVI: dCTP deaminase

clearly distinguishable, hepatocytes were neatly arranged, only slight edema was observed in a few hepatocytes, and hemorrhage foci and inflammatory infiltration were essentially absent. In the 10^7PFU group, hepatocellular morphology was also close to normal, the inflammatory response subsided significantly, and liver histological morphology was similar to that of the control group.

The boundary between red and white pulp was distinct, with regularly shaped lymphoid follicles (containing intact germinal centers) in the white pulp and normal splenic cord and sinus structures in the red pulp. At 3 days post-phage treatment, the 10^7PFU group exhibited lymphoid follicle hyperplasia in the splenic white pulp (with disorganized structure in some follicles), along with diffuse inflammatory cell infiltration (predominantly neutrophils and mononuclear macrophages) and marked splenic sinus congestion in the red pulp. In the 10^8PFU group, although reactive lymphoid tissue hyperplasia and inflammatory infiltration in the red pulp were noted, the lesion severity was milder than in the 10^7PFU group. By 7 days post-treatment, the boundary between red and white pulp in the 10^8 PFU group gradually became distinct, lymphoid follicle contours returned to normal, inflammatory cell infiltration in the red pulp was significantly reduced, and splenic sinus congestion was alleviated. In the 10^7PFU group, splenic lymphoid tissue morphology was further repaired, the range of inflammatory cell infiltration narrowed, and histological structure approached normal.

In the control group, glomerular structure was normal, with no dilation or stenosis of glomerular capillary loops. Renal tubular epithelial cells were tightly arranged with regular morphology, no renal tubular lumen dilation was observed, and no congestion, hemorrhage, or inflammatory cell infiltration was present in the renal interstitium. At 3 days post-phage treatment, the 10^7 PFU group showed renal tubular epithelial cell degeneration and necrosis, dilation of some renal tubular lumens, and cast formation due to epithelial cell shedding into the lumens, accompanied by focal hemorrhage and a small number of neutrophils infiltrating the renal interstitium. In the 10^8 PFU group, renal tubular epithelial cell damage was milder, with only focal epithelial cell edema and limited renal interstitial hemorrhage and inflammatory infiltration. By 7 days post-treatment, renal tubular epithelial cells in the 10^8 PFU group were neatly arranged, lumen morphology returned to normal, epithelial cell degeneration and necrosis disappeared, and renal interstitial hemorrhage and inflammatory infiltration completely subsided. In the 10^7 PFU group, renal tubular structure was basically restored, epithelial cell morphology was normal, and renal interstitial pathological changes were significantly alleviated.

S. aureus infection caused varying degrees of pathological damage to the liver, spleen, and kidneys of mice. After treatment with phage vB_Sau_SHZU01, tissue damage was gradually repaired over time. At 3 days post-treatment, damage was more severe in the low-titer group (10^7 PFU) and milder in the high-titer group (10^8 PFU), indicating that high-titer phage provided stronger early protection. By 7 days post-treatment, damage in both groups was significantly repaired with morphology close to normal, suggesting that sufficient tissue repair could also be achieved in the low-titer group with prolonged treatment. These results demonstrate that this phage effectively alleviates *S. aureus*-induced pathological damage in the liver, spleen, and kidneys, and that both phage titer and treatment duration jointly regulate the tissue repair process.

Antibacterial activity of phage vB_SauL_SHZU01 in dairy products: The antibacterial efficacy of phages against *S. aureus* was synergistically regulated by temperature, dairy matrix, and multiplicity of infection (MOI), as depicted in Fig. 6A-F. At 4°C, phages exhibited negligible antibacterial activity in raw milk (Fig. 6A), where *S. aureus* CFU remained stable over 24 h, while in yogurt (Fig. 6B), phages effectively reduced *S. aureus* load, with higher MOIs (e.g., MOI = 100, 10) showing more pronounced inhibition. At 25°C, *S. aureus* proliferated vigorously in raw milk (Fig. 6C), and phages failed to suppress their growth, whereas in yogurt (Fig. 6D), phages maintained potent antibacterial activity, and *S. aureus* CFU decreased continuously in a MOI-dependent manner. At 37°C, raw milk (Fig. 6E) supported transient *S. aureus* growth followed by a mild decline under high-MOI phage treatment, while yogurt (Fig. 6F) displayed dynamic, MOI-dependent responses: high MOIs (e.g., MOI = 100) reduced *S. aureus* CFU to approximately 5 log CFU by 12 h, followed by a significant rebound to ~9 log CFU at 24 h, whereas low MOIs (e.g., MOI = 0.01) resulted in sustained low CFU

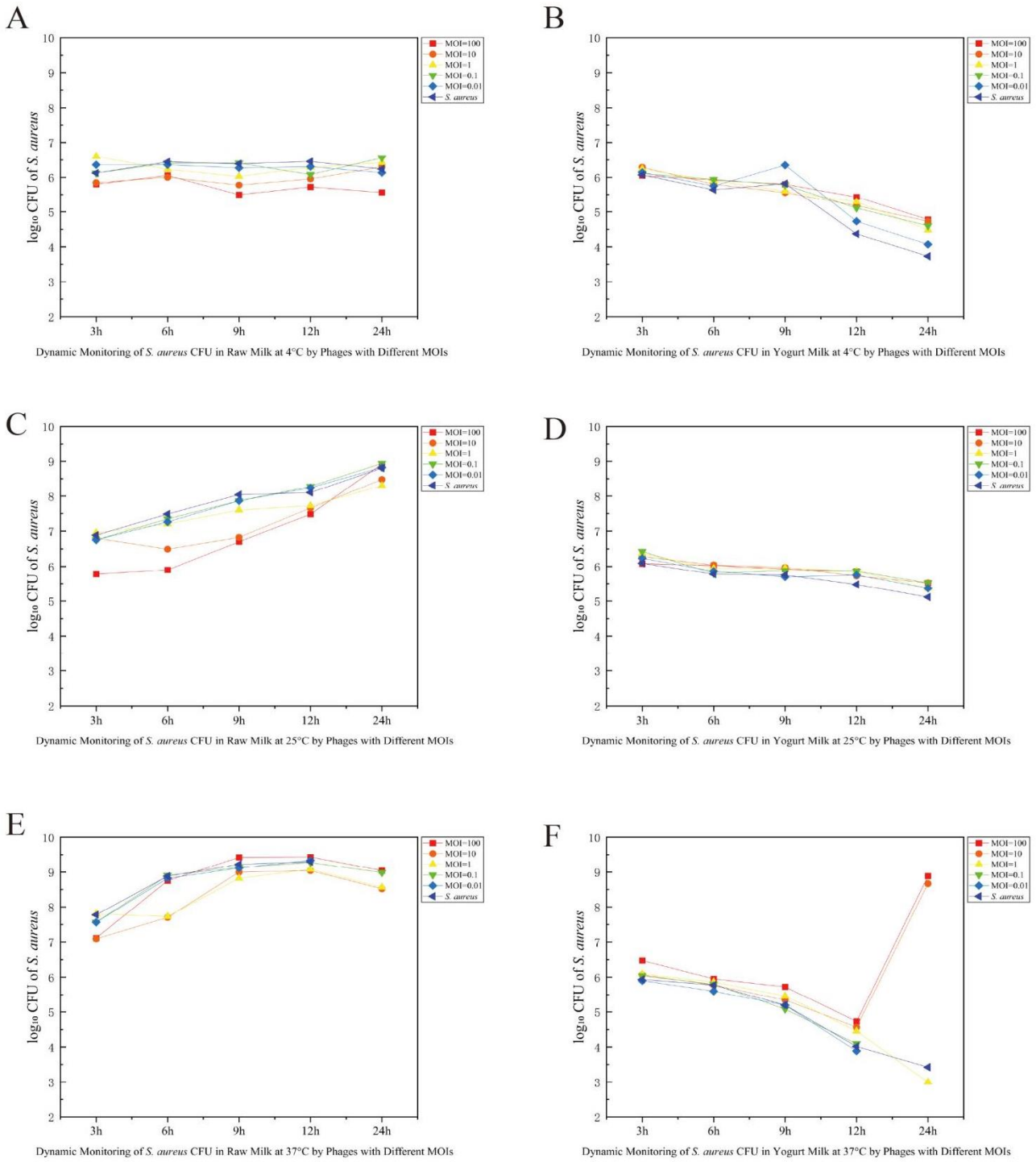

Fig. 6: The effects of different temperatures (4, 25 and 37°C), dairy matrices (raw milk, yogurt), and phage multiplicities of infection (MOI) on the dynamic changes of *S. aureus* $\log_{10}$ CFU. Panels A, C, and E correspond to the 24-hour dynamic monitoring of *S. aureus* $\log_{10}$ CFU in raw milk under 4, 25 and 37°C, respectively, following treatment with phages at different MOIs; Panels B, D, and F correspond to the 24-hour dynamic monitoring of *S. aureus* $\log_{10}$ CFU in yogurt under the same temperature conditions with phages at different MOIs. All data were determined by the colony-forming unit (CFU) assay and subjected to $\log_{10}$ transformation, aiming to elucidate the synergistic regulatory effects of temperature, dairy type, and phage MOI on the growth of *S. aureus*.

levels (reaching ~3 log CFU at 24 h) rather than bacterial resurgence. Notably, yogurt consistently outperformed raw milk in facilitating phage-mediated *S. aureus* inhibition across all tested temperatures, likely due to its acidic environment and unique matrix composition. Collectively, high MOIs (≥10) were critical for robust antibacterial efficacy, and yogurt at 25-37 °C emerged as the most favorable system for phage-based *S. aureus* control in dairy products.

DISCUSSION

S. aureus infection in dairy cattle is a significant challenge faced by cattle farms, as it leads to a substantial decline in milk production. Furthermore, the quality of the milk produced may pose risks to human health, resulting in a considerable economic burden for farmers. Additionally, due to its potential as a zoonotic disease, such infections have attracted global attention (Cosandey

et al., 2016). The transfer of antimicrobial resistance genes and virulence factors from animals to humans could exacerbate the severity of certain infectious diseases (Naranjo-Lucena *et al.*, 2025). As a result, there is growing interest in the rational use of antibiotic alternatives for treating bovine-derived *S. aureus* infections (Molineri *et al.*, 2021). In the present study, a bacteriophage targeting multidrug-resistant *S. aureus* was isolated, and its biological characteristics were systematically analyzed. The phage's antibacterial activity and anti-biofilm properties were evaluated, and a mouse infection model was established to assess its therapeutic effect *in-vivo*. Additionally, the bacteriostatic effect of the phage in various dairy products was examined, and its potential for practical application in dairy-related industries was explored.

In this study, the phage vB_SauL_SHZU01, which targets bovine-derived *S. aureus*, was successfully isolated. Transmission electron microscopy (TEM) observations revealed that this phage exhibits a typical structural morphology, consisting of an icosahedral head and a long tail, which is characteristic of certain phage families, such as Myoviridae. Previous studies have demonstrated that the growth curve (*i.e.*, infection cycle) of phage vB_SauL_SHZU01 serves as a key indicator of its replication capacity, characterized by a short latent period (only 30 minutes) and robust infectivity. A shorter latent period suggests a faster replication rate, and replication efficiency is closely linked to the phage's burst size. A larger burst size during the phage life cycle correlates with higher phage productivity, as more progeny phages are produced per infection cycle. This characteristic further enhances its potential for use in phage therapy (Ge *et al.*, 2020).

In terms of environmental adaptability, phage vB_SauL_SHZU01 demonstrates excellent low-temperature stability, remaining stable between 4°C and 50°C. However, its titer gradually decreases as the temperature rises to 60°C, with a significantly accelerated decline at 70°C. From an application standpoint, its stability at low temperatures allows for short-term storage at conventional refrigeration temperatures (4°C), eliminating the need for complex freezing equipment. This significantly reduces storage costs for both laboratory research and field applications. While its activity decreases at higher temperatures, its tolerance up to 50°C remains compatible with the typical temperature range encountered on cattle farms during summer, which will not unduly limit its potential for field use.

Analysis of the pH stability of phage vB_SauL_SHZU01 revealed that it retains high activity only within the pH range of 6-10 and is completely inactivated under strongly acidic (pH 1-4) or strongly alkaline conditions (pH 11-14). This indicates that the phage has a narrow pH adaptability and a strong dependence on a neutral environment. The application value of this characteristic should be considered in relation to target scenarios. On one hand, the pH ranges of key microenvironments, such as the dairy cow mammary ducts (pH 6.2-7.4) and the middle section of the intestine (pH 6.5-7.8), closely align with the optimal pH range for this phage, suggesting that it can maintain its activity in interventions targeting mastitis or intestinal MRSA infections. On the other hand, its limited pH adaptability may restrict its use in extreme environments. For instance, when combined with acidic disinfectants (e.g., peracetic acid) or alkaline cleaners, the phage may be inactivated due to pH levels exceeding its tolerance range. Therefore, such combinations should be avoided in application protocols, or environmental pH should be regulated using buffer systems to preserve its activity (Imklin *et al.*, 2023).

Studies have shown that the optimal multiplicity of infection (MOI) for vB_SauL_SHZU01 is 0.1. This MOI is associated with a short latent period (0-20 minutes), a rapid lysis period (20-80 minutes), and stable progeny release, which are key advantages for its potential use as an agent for controlling *S. aureus*. From a practical application standpoint, the finding that the optimal MOI is 0.1 provides clear guidance: in subsequent *in-vitro* bacteriostatic or *in-vivo* therapeutic experiments, the concentration can be adjusted based on a phage-to-bacteria ratio of 0.1:1, ensuring efficient proliferation and lysis with minimal dosage, thus reducing application costs. Moreover, the short latent and lysis periods enable the phage to rapidly complete the "adsorption-invasion-proliferation-release" cycle. Compared to previously reported anti-MRSA phages (e.g., vB_SauP_ASUmrsa123, which has a latent period of approximately 55 minutes and an estimated burst size of 167 PFU (El-Tawab *et al.*, 2014), vB_SauL_SHZU01 inhibits bacterial proliferation more quickly. This makes it particularly suitable for emergency intervention in acute MRSA infections, such as dairy cow acute mastitis, by reducing bacterial colonization and minimizing damage to the host. Phage vB_SauL_SHZU01 demonstrates poor stability when exposed to ultraviolet (UV) radiation, with a significant reduction in activity as exposure time increases. The underlying mechanism may involve UV-induced damage to the phage's DNA-UV radiation, particularly at a wavelength of 254nM, can induce the formation of pyrimidine dimers in the phage genome. This disrupts the structural integrity of the DNA, inhibiting its replication and lytic functions (Jacob *et al.*, 2025). From a practical application standpoint, this characteristic highlights the need for optimized storage and usage conditions. UV exposure should be avoided during storage, and the use of light-proof containers or packaging is recommended. In outdoor settings, such as dairy farms, phage application should be performed on cloudy days or in the evening. Alternatively, UV resistance could be enhanced through formulation optimization, such as the inclusion of UV protectants like bovine serum albumin and chitosan, to prevent activity loss due to UV radiation and ensure the efficacy of the phage in prevention and control.

In summary, the biological characteristics of phage vB_SauL_SHZU01 present both advantages and limitations. Its low-temperature stability, adaptability to neutral environments, low optimal multiplicity of infection (MOI), and short latent and lytic periods confer significant potential for low-temperature storage of bovine-derived MRSA, targeted *in-vivo* intervention, and efficient lysis. However, its sensitivity to high temperatures, narrow pH adaptation range, and instability under UV radiation warrant further technical optimization

(e.g., addition of stabilizers, adjustment of buffer systems, and development of light-proof formulations) to improve its practical application.

The genomic characteristics of phage vB_SauL_SHZU01 provide a fundamental molecular basis for analyzing its biological functions and evaluating its potential for application. Its genome consists of a linear double-stranded DNA structure, 44,364 bp in length, with a GC content of 33.6%. This GC content is highly consistent with that of several previously reported *Staphylococcus aureus* (*S. aureus*) phages (Zhang *et al.*, 2022), suggesting that the phage has developed an adaptive genomic relationship with its host through long-term co-evolution. In comparison, phage SauPS-28, which is also capable of lysing methicillin-resistant *S. aureus* (Zhao *et al.*, 2024), has a genome length of 43,286 bp and a GC content of 31.03%. Both phages exhibit genome sizes and GC contents within the typical range for *S. aureus* phages, reflecting the consistency of species-specific genomic traits. Sixty-one open reading frames (ORFs) were predicted in the genome of vB_SauL_SHZU01. In contrast, genomic functional annotation of phage MetB16-another phage capable of lysing methicillin-resistant *S. aureus*-identified 72 ORFs, 34 of which encode hypothetical proteins with unknown functions (Erdoğdu *et al.*, 2025). The ORF counts for both phages are comparable, reflecting the typical coding sequence features of Staphylococcus phage genomes. Both also contain genes of unknown function, highlighting the complexity of functional differentiation within phage genomes. The functional genomic modules of vB_SauL_SHZU01-including those responsible for lysis, replication, regulation, integration, assembly, and infection-are clustered, with most genes transcribed in the same direction. This gene distribution aligns with the typical organization of phages, where coordinated gene expression is mediated through operon structures. Such an arrangement efficiently supports the complete “infection-replication-lysis” lifecycle, providing a molecular foundation for the phage's high proliferation efficiency (Azam *et al.*, 2019).

In terms of functional module organization, the tail fiber protein-encoding gene within the infection module is responsible for host targeting specificity and plays a crucial role in the phage’s adsorption to *S. aureus*. Lysozyme-related genes in the lysis module, such as the SPP1 phage perforin homolog vB_SauL_SHZU01_24, mediate the degradation of the host cell wall, ensuring efficient release of progeny phages. The DNA polymerase family A gene and the DNA-binding protein gene in the replication module work synergistically to facilitate rapid genomic amplification. Meanwhile, the transcription regulatory factor gene and the anti-repressor protein (Ant) gene in the regulation module coordinate the temporal expression of genes throughout the various stages of phage proliferation. This clear division of functional modules and coordinated gene expression constitutes the core molecular foundation for the phage to maintain stable antibacterial activity in complex environments, such as dairy matrices (Yehl *et al.*, 2019).

Furthermore, the identification of an anti-CRISPR protein-encoding region (Stanley *et al.*, 2018) indicates that vB_SauL_SHZU01 can synthesize anti-CRISPR proteins. These proteins specifically counteract the *S. aureus* CRISPR-Cas immune system, thereby significantly enhancing the phage’s infection success rate and proliferation efficiency. This unique characteristic provides an advantage over phages lacking this system, particularly when targeting *S. aureus* strains with functional CRISPR-Cas systems. This trait makes vB_SauL_SHZU01 particularly suitable for applications in environments such as dairy products, where host organisms are prone to activating immune defense mechanisms. Notably, all multidrug-resistant, biofilm-forming *S. aureus* strains consistently harbor the ica gene cluster (*icaA*, *icaB*, *icaC*, *icaD*), its regulatory factor *icaR*, and the genes encoding clumping factors A and B (*clfA*, *clfB*) (Noumi *et al.*, 2025). These genes are critical for biofilm formation and virulence in such strains. Virulence-related gene annotation reveals that vB_SauL_SHZU01's genome contains the *fimB* and *clpP* genes, which are likely acquired through horizontal gene transfer from *S. aureus*. The *fimB* and *clpP* genes identified in this study are hypothesized to be involved in the initial phage-host cell interaction and the regulation of host protein degradation, respectively. These genes provide important targets for further investigation into the molecular mechanisms underlying phage-*S. aureus* interactions (Ranjith *et al.*, 2020).

This study provides experimental evidence for the individualized adjustment of the "dose-course" in phage therapy. For severe infections, high-titer regimens, such as 10^8 PFU, should be prioritized to shorten the inflammatory window, aligning with the therapeutic principle of "rapidly controlling pathogenic bacterial load" in acute infections. For mild infections or preventive applications, a 10^7 PFU regimen combined with an extended treatment course can achieve comparable therapeutic outcomes, reducing both formulation costs and potential immunostimulation risks. This strategy closely mirrors the approach of "adjusting phage dose according to infection severity" used in the treatment of multidrug-resistant Serratia marcescens infections, as reported by Duan *et al.* (2025), with the core focus on balancing phage proliferation kinetics and bacterial clearance needs. Additionally, the observed repair effect of phages on kidney tissue in this study holds particular significance. *S. aureus* infection is frequently associated with complications such as renal abscesses and renal tubular necrosis, mechanisms of which involve bacterial colonization of renal tubular epithelial cells, activation of the complement system, and deposition of immune complexes (Satoskar *et al.*, 2020). In this study, 7 days after treatment with 10^8 PFU of phages, degenerative necrosis of renal tubular epithelial cells had fully subsided, and renal interstitial inflammation had resolved. This suggests that vB_SauL_SHZU01 can not only clear circulating *S. aureus* but also target local renal infection sites. These findings offer a new potential avenue for phage therapy in treating *S. aureus*-associated nephropathy. Treatment with SapYZU15 resulted in faster tissue healing, reduced weight loss, and decreased numbers of viable *S. aureus* in the mouse abscess model. In addition, prophylaxis with SapYZU15 effectively inhibits abscess formation through a synergistic effect with proinflammatory cytokines (Wen *et al.*, 2023). It is

important to note several limitations of this study. First, the mouse model used in this study represents an acute infection model, which differs from the chronic *S. aureus* infection processes seen in clinical conditions (e.g., osteomyelitis and endocarditis).

This study demonstrates that the inhibitory effect of bacteriophages against *S. aureus* in dairy products results from the synergistic interaction between temperature, matrix type, and multiplicity of infection (MOI), with particular emphasis on the advantages of the yogurt matrix and the necessity for a high MOI. The yogurt matrix was compatible with bacteriophage activity across all tested temperatures, likely due to the acidic environment created during yogurt fermentation. Bacteriophages can maintain stable activity over a broad pH range (e.g., pH 4-10) (Imklin *et al.*, 2023). Specifically, Imklin *et al.* (2023) found that the acidic environment enhances bacteriophage adsorption efficiency by altering the cell membrane permeability of *S. aureus*, while also inhibiting the metabolic enzyme activity of the bacterium, thus forming a "dual inhibitory" effect. In contrast, the neutral environment of raw milk promotes the rapid proliferation of *S. aureus*, thereby weakening the bacteriophage's infective advantage. This aligns with the findings in Pujato's (2019) review on the regulation of bacteriophage activity by dairy matrices.

The regulatory role of temperature is evident in the significant enhancement of bacteriophage proliferation rates at moderate to high temperatures (25-37°C). Larcom and Thaker (1977) confirmed this in their study of the phi29 bacteriophage, where the latent period was stable, and the burst size was considerable at 37°C. Additionally, Blazanin *et al.* (2022) demonstrated in their study of the therapeutic phage OMKO1 that an optimal temperature range (28-37°C) reduces bacteriophage particle damage, shortens the lysis cycle, and aligns the phage's activity with the logarithmic growth phase of *S. aureus*. This helps explain the significant reduction in *S. aureus* CFU to below detection limits in the high MOI yogurt group at 37°C observed in the present study. In contrast, low temperatures (4°C) inhibit both bacteriophage activity and bacterial metabolism. Nascimento *et al.* (2022) also observed that *S. aureus* growth in raw milk stagnates under refrigerated conditions in their study of the UFJF_PfDIW6 bacteriophage. While bacteriophage activity is reduced, indirect bacterial control can still be achieved through the persistence of the phages, with a combined application reducing pathogenic bacteria in refrigerated milk by 3 log CFU/mL.

The MOI dose effect is particularly pronounced in complex dairy systems. A high MOI (≥10) can quickly saturate the surface receptors of *S. aureus* through "saturating adsorption," reducing the likelihood of bacterial resistance development (Tan *et al.*, 2024). In contrast, pathogenic bacterial rebound observed in the low MOI (≤0.01) group in yogurt at 37°C may be associated with insufficient phage infection pressure, allowing gradual bacterial adaptation and resistance. A similar phenomenon was observed with the dairy-derived phage Hesat, isolated by Turchi *et al.* (2024), which failed to sustain *S. aureus* inhibition when treated with a low MOI. As core matrix components in dairy products, milk proteins and fats coordinately regulate the proliferation efficiency and antibacterial activity of bacteriophages through distinct action mechanisms. Among these, milk proteins such as casein and whey protein can be adsorbed and encapsulate phages to form protective barriers, which mitigate the damage to phage capsids caused by low pH and proteases and thus improve phage survival capacity; meanwhile, they act as auxiliary nutrients to promote the replication of phages in host bacteria and enhance lytic activity. In contrast, fat globules in dairy products form spatial barriers that hinder the contact and binding between phages and *S. aureus*, thereby reducing phage infection efficiency. Notably, the fat globules in fermented yogurt exhibit a more compact structure, leading to a weaker spatial barrier effect compared with raw milk. In addition, the ratio and existing form of milk proteins and fats further coordinately regulate the kinetics of phage-bacterium interactions. In the yogurt system, the protective effect of milk proteins may effectively counteract part of the spatial barrier effect of fats, which is also one of the important reasons why the antibacterial activity of phages in yogurt is superior to that in raw milk.

Conclusions: To address the demand for biological control of bovine-derived methicillin-resistant *S. aureus* (MRSA), this study systematically completed the isolation, identification, phenotypic characterization, *in-vivo* therapeutic validation and genomic analysis of phage vB_SauL_SHZU01, providing key experimental evidence for the prevention and control of MRSA hazards in the livestock industry. This phage possessed superior phenotypic traits including excellent low-temperature stability, a low optimal MOI and a short latent period. *In-vivo* mouse experiments confirmed the existence of its effective therapeutic dosage threshold: a high dosage achieved a 100% survival rate in infected mice and promoted the repair of pathological damage in the liver, spleen and kidney. At the genomic level, no antimicrobial resistance genes were detected, and the phage harbored an anti-CRISPR system, which laid a molecular foundation for its safe and efficient application. This study also identified the limitations of the phage: it was sensitive to high temperatures and ultraviolet radiation and had a narrow pH adaptation range; numerous genes with unknown functions and its latent lysogenic potential in the genome awaited further in-depth verification. In summary, phage vB_SauL_SHZU01 is a novel candidate agent for the control of bovine-derived *S. aureus*, and its phenotypic traits as well as *in-vivo* effective dosage parameters provide an important reference for the subsequent development of targeted formulations and the formulation of clinical administration protocols. In the future, if this phage is translated into practical application, standardized purification processes will be adopted to remove impurities and systematic food safety evaluation experiments will be conducted; additionally, formulation optimization, the design of targeted delivery systems and multi-omics functional validation will further unlock its translational application value in dairy product preservation and the prevention and control of *S. aureus* infections in livestock and poultry.

Authors contributions: YL: Investigation, Methodology, Data curation, Software, Writing-original draft; WW:

Investigation, Methodology, Data curation; YG: Investigation, Software, Data collection; JW: Investigation, Data curation; MT: Investigation, Data collection; HZ: Writing-review & editing, Supervision; HH: Conceptualization, Methodology, Data curation, Writing-review & editing, Supervision, Funding acquisition.

Declaration of competing interest: The authors declare that they have no known competing financial interests or non-financial interests (such as personal or professional relationships, affiliations, or commitments) that could reasonably be perceived as influencing the preparation, conduct, or reporting of the work presented in this paper. For data availability, all data supporting the findings of this study will be made available to qualified researchers upon reasonable request.

Data availability: The whole-genome sequencing data of the clinically isolated multidrug-resistant *S. aureus* strain are available at NCBI SRA under the accession number PRJNA1417252, and the whole-genome sequencing data of phage vB_SauL_SHZU01 are available at NCBI SRA under the accession number PX974351.

Ethics approval and consent to participate: All animal experimental procedures used in this study were approved by the Institutional Animal Care and Use Committee of Shihezi University (No. A2025-1204) (Shihezi, China).

Consent for publication: Not applicable.

Funding: This work was supported by the Key Science and Technology Development Project of Xinjiang Production and Construction Corps 2024 (Grant No. 2024AB034): Research and Demonstration of Rapid Diagnostic Technologies for Drug-Resistant Bacteria in Bovine Reproductive Tract.

REFERENCES

Abebe AA and Birhanu AG, 2023. Methicillin resistant *Staphylococcus aureus*: molecular mechanisms underlying drug resistance development and novel strategies to combat. Infection and Drug Resistance 16:7641-7662.

Azam AH and Tanji Y, 2025. Peculiarities of *Staphylococcus aureus* phages and their possible application in phage therapy. Applied Microbiology and Biotechnology 103(11):4279-4289.

Badawy B, Elafify M, Farag AMM, *et al*., 2022. Ecological distribution of virulent multidrug-resistant *Staphylococcus aureus* in livestock, environment, and dairy products. Antibiotics (Basel) 11(11):1651.

Blazanin M, Lam WT, Vasen E, *et al*., 2022. Decay and damage of therapeutic phage OMKO1 by environmental stressors. PLoS One 17(2):e0263887. doi: 10.1371/journal.pone.0263887.

Chambers HF and Fowler VG Jr, 2024. Intertwining clonality and resistance: *Staphylococcus aureus* in the antibiotic era. Journal of Clinical Investigation 134(19):e185824.

Cosandey A, Boss R, Luini M, *et al*., 2016. *Staphylococcus aureus* genotype B and other genotypes isolated from cow milk in European countries. Journal of Dairy Science 99(1):529-40.

Duan X, Liu W, Xiao Y, *et al*., 2025. Exploration of the feasibility of clinical application of phage treatment for multidrug-resistant *Serratia marcescens*-induced pulmonary infection. Emerging Microbes and Infection 14(1):2451048.

Erdoğdu B, Dokuz S, Güngör G, *et al*., 2025. Novel MRSA-targeting phage MetB16: Genomic features, structural insights, and therapeutic applications. Turkish Journal of Biology 49(3):292-308.

El-Tawab AKA, Othman BA, Sharaf A, *et al*., 2024. Characterization and complete genome sequence of highly lytic phage active against methicillin-resistant *Staphylococcus aureus* (MRSA) isolated from Egypt. Virology Journal 21(1):284.

Ge H, Hu M, Zhao G, *et al*., 2020. The "fighting wisdom and bravery" of tailed phage and host in the process of adsorption. Microbiology Research 230:126344.

Guzmán-Luna P, Nag R, Martínez I, *et al*., 2022. Quantifying current and future raw milk losses due to bovine mastitis on European dairy farms under climate change scenarios. Science of the Total Environment 833:155149.

Imklin N, Chaengphaniad P, Šimoliūnas E, *et al*., 2023. A novel Staphylococcus phage, vB_Sau-RP15, and its application in contaminated milk. Letters in Applied Microbiology 76(1):ovac003.

Jacob MF, Quiberoni ADL, Ballari MLM, *et al*., 2025. Kinetic modeling of dairy phages inactivation under UV-C irradiation. Science of the Total Environment 983:179664.

Kim SG, Giri SS, Yun S, *et al*., 2020. Synergistic phage-surfactant combination clears IgE-promoted *Staphylococcus aureus* aggregation *in-vitro* and enhances the effect *in-vivo*. International Journal of Antimicrobial Agents 56(1):105997.

Larcom LL and Thaker NH, 1997. The effects of temperature and ultraviolet irradiation on multiplication of bacteriophage phi29. Biophysics Journal 19(3):299-306. doi: 10.1016/S0006-3495(77)85589-6.

Lei B, Mu J, Xu G, *et al*., 2024. Jing-Yin-Gu-Biao formula protects mice from postinfluenza *Staphylococcus aureus* infection by ameliorating acute lung injury and improving hypercoagulable state via inhibiting NETosis. Frontiers in Immunology 16:1567522.

Leprince A and Mahillon J, 2023. Phage adsorption to gram-positive bacteria. Viruses 15(1):196.

Liu K, Wang C, Zhou X, *et al*., 2024. Bacteriophage therapy for drug-resistant *Staphylococcus aureus* infections. Frontiers in Cellular Infections and Microbiology 14:1336821.

Imklin N, Chaengphaniad P, Šimoliūnas E, *et al*., 2023. A novel Staphylococcus phage, vB_Sau-RP15, and its application in contaminated milk. Letters in Applied Microbiology 76(1):ovac003.

Mobarezi Z, Esfandiari AH, Abolbashari S, *et al*., 2025. Efficacy of phage therapy in controlling staphylococcal biofilms: a systematic review. European Journal of Medical Research 30(1):605.

Molineri AI, Camussone C, Zbrun MV, *et al*., 2021. Antimicrobial resistance of *Staphylococcus aureus* isolated from bovine mastitis: Systematic review and meta-analysis. Preventive Veterinary Medicine 188:105261.

Nascimento ECD, Sabino MC, Corguinha LDR, *et al*., 2022. Lytic bacteriophages UFJF_PfDIW6 and UFJF_PfSW6 prevent *Pseudomonas fluorescens* growth *in-vitro* and the proteolytic-caused spoilage of raw milk during chilled storage. Food Microbiology 101:103892.

Naranjo-Lucena A, Becker P, Madigan G, *et al*., 2025. Longitudinal patterns in the isolation and antimicrobial resistance of bovine mastitis-causing bacteria in Ireland. Antibiotics (Basel) 14(3):243.

Nie X, Tong Y, Li M, Ning Z, *et al*., 2025. Bacteriophage therapy for critical antibiotic-resistant Gram-positive bacteria: A systematic review of clinical researche. Microbiology Research 298:128231.

Noumi E, Zmantar T, Bouali N, *et al*., 2025. Whole-genome sequencing and biofilm gene characterization in multidrug-Resistant *Staphylococcus aureus* clinical strains. Journal of Genetic Engineering and Biotechnology 23(3):100521.

Phiri BSJ, Hang'ombe BM, Mulenga E, *et al*., 2022. Prevalence and diversity of *Staphylococcus aureus* in the Zambian dairy value chain: A public health concern. International Journal of Food Microbiology 375:109737.

Pujato SA, Quiberoni A, Mercanti DJ, 2019. Bacteriophages on dairy foods. Journal of Applied Microbiology 126(1):14-30.

Ranjith K, SaiAbhilash CR, Sai Prashanthi G, *et al*., 2020. Phylogenetic grouping of human ocular *Escherichia coli* based on whole-genome sequence analysis. Microorganisms 8(3):422.

Satoskar AA, Parikh SV, Nadasdy T, 2020. Epidemiology, pathogenesis, treatment and outcomes of infection-associated glomerulonephritis. Nature Reviews in Nephrology 16(1):32-50.

Schooley RT, 2024. Translational research priorities for bacteriophage therapeutics. Essays in Biochemistry 68(5):621-631.

Stanley SY, Maxwell KL, 2018. Phage-encoded anti-CRISPR defenses. Annual Reviews in Genetics 52:445-464.

Swets MC, Bakk Z, Westgeest AC, *et al*., 2024. Clinical subphenotypes of *Staphylococcus aureus* bacteremia. Clinical and Infectious Diseases 79(5):1153-1161.

Tan X, Chen K, Jiang Z, *et al*., 2024. Evaluation of the impact of repeated intravenous phage doses on mammalian host-phage interactions. Journal of Virology 98(1):e0135923.

Turchi B, Campobasso C, Nardinocchi A, *et al*., 2024. Isolation and characterization of novel *Staphylococcus aureus* bacteriophage Hesat from dairy origin. Applied Microbiology and Biotechnology 108(1):299. doi: 10.1007/s00253-024-13129-y.

Velasco Garcia WJ, Araripe Dos Santos Neto N, Borba Rios T, *et al*., 2025. Genetic basis of antibiotic resistance in bovine mastitis and its possible implications for human and ecological health. Critical Reviews in Microbiology 51(3):427-440.

Wang W, Lin X, Jiang T, *et al*., 2018. Prevalence and characterization of *Staphylococcus aureus* cultured from raw milk taken from dairy cows with mastitis in Beijing, China. Frontiers in Microbiology 9:1123.

Wang Y, Zhang P, Wu J, *et al*., 2023. Transmission of livestock-associated methicillin-resistant *Staphylococcus aureus* between animals, environment, and humans in the farm. Environmental Science and Pollution Research International 30(37):86521-86539.

Wen H, Zhou W, Wu Y, *et al*., 2023. Effective treatment of a broad-host-range lytic phage SapYZU15 in eliminating *Staphylococcus aureus* from subcutaneous infection. Microbiology Research 276:127484.

Yehl K, Lemire S, Yang AC, *et al*., 2019. Engineering phage host-range and suppressing bacterial resistance through phage tail fiber mutagenesis. Cell 179(2):459-469.e9.

Zhang L, Shahin K, Soleimani-Delfan A, *et al*., 2022. Phage JS02, a putative temperate phage, a novel biofilm-degrading agent for *Staphylococcus aureus*. Letters in Applied Microbiology 75(3):643-654.

Zhao P, Zhao W, Zhai X, *et al*., 2024. Biological characterization and genomic analysis of a novel methicillin-resistant *Staphylococcus aureus* phage, SauPS-28. Microbiology Spectrum 12(2):e0029523.